Catal Lett (2008) 126:426–435
DOI 10.1007/s10562-008-9648-5

Oxidative Dehydrogenation of Ethane over Ce-based Monolithic Catalysts using CO_2 as Oxidant

Xuejun Shi · Shengfu Ji · Kai Wang · Chengyue Li

Received: 6 August 2008 / Accepted: 8 September 2008 / Published online: 11 October 2008

Abstract Highly active Ce-based monolithic catalysts for oxidative dehydrogenation of ethane with CO_2 were prepared and characterized by various techniques. The high oxidation state Ce^{4+} species had higher catalytic activity than the Ce^{3+} species in the monolithic catalysts. The Ce^{4+} species was reduced to Ce^{3+} species in the ethane dehydrogenation process, and the reduced Ce species was reoxidized to the Ce^{4+} species by treatment with CO_2 at 750 °C, the Ce redox cycle played an important role in the catalyst's high activity.

Keywords Monolithic catalyst · Cerium oxide · Dehydrogenation · CO_2 · XPS

1 Introduction

Oxidative dehydrogenation (ODH) or non-ODH of ethane into ethylene is an industrially important process due to the increased demand of ethylene [1]. Catalytic dehydrogenation is accepted as a method for the production of ethylene more selectively even at higher conversion. Carbon dioxide has been thought to be a possible substitute for oxygen. The introduction of CO_2 in the catalytic dehydrogenation of ethane has many potential advantages. First, thermodynamic equilibrium limitation is overcome and ethylene yield is improved by removal of hydrogen ($CO_2 + H_2 \rightarrow CO + H_2O$); second, deep oxidation that occurred as a result of using oxygen as oxidant is avoided; third, it realizes the recycling of greenhouse gas CO_2 when used as a soft oxidant.

Supported chromium oxides are well known to be active catalysts for the ODH reaction [2]. However, the use of Cr-based catalysts, especially working at high temperature is banned in several countries, for the known environmental problems. So, from the sustainability point of view, it is necessary to find a substitute for the Cr-based catalyst. Recently, cerium oxide has attracted much attention as catalyst, either as an effective promoter or as a supporting material based on its high oxygen-storage capacity and facile oxidation/reduction of the Ce^{4+}/Ce^{3+} redox cycle. As is well known, the catalyst performance depends on a number of factors, such as the chemical nature of the active oxygen species, the redox properties and the acid–base character, which in turn depend on transition metal loading, dispersion and support effects [3–6]. Mesoporous silica SBA-15 [7, 8], which has highly ordered hexagonal structure with high surface areas of 600–1,000 m^2/g, adjustable pore sizes of 4.6–30 nm and wall thickness of 3.1–6.4 nm, has attracted wide attention as a new material for catalysts and catalyst supports. It has been reported that Ce-based catalysts supported on SBA-15 exhibit excellent activity for the dehydrogenation of ethylbenzene to styrene with CO_2 [9], which has been attributed to the high degree of dispersion of active phase within the channels of SBA-15. So the studies of cerium species introduced into SBA-15 would be useful in developing Ce-containing catalysts with desirable catalytic properties.

Conventional catalysts in the form of pellets or granules have some disadvantages when used in commercial catalytic reactors, since their use results in high pressure drops across the catalyst bed and high temperature gradients in the reactor. Recently, monolithic catalysts, especially that using the metal as the catalyst supports, have gained

X. Shi · S. Ji (✉) · K. Wang · C. Li
State Key Laboratory of Chemical Resource Engineering, Beijing University of Chemical Technology, 15 Beisanhuan Dong Road, P.O. Box 35, Beijing 100029, China
e-mail: jisf_buct@live.cn

considerable attention [10, 11]. The catalysts can provide some suitable order flow channels in many forms according to reactor types; even can be made into monolithic catalytic reactors with honeycomb structure. Comparing with conventional fixed-bed reactors with pellet or powder catalysts, those using metallic monolithic catalysts have lower pressure drop, high heat and mass transfer rates and minimum axial dispersion arising from the uniquely structured multi-channel configuration of monoliths [12, 13]. Liu et al. [14, 15] study results indicated that monolithic catalysts also had other advantages over conventional powdered catalyst reactors, such as the possibility of using high flow rate, ease of scale-up, and in some cases, selectivity enhancement.

In this paper, a series of Ce-based monolithic catalyst using FeCrAl alloy as support were prepared, and the activity Ce species were characterized using XRD, TPR, and XPS analysis. The aim of this work is to understand the redox cycle of the highly activity Ce species with ethane and CO_2, an area that had not been studied before. Our studies include the determination of activation energies to clarify the importance of individual redox steps and the potential application of Ce-based monolithic catalyst in the ODH reaction.

2 Experimental Section

2.1 Catalyst Preparation

SBA-15 was synthesized according to the method described in the literature [7]. The Ce/SBA-15 samples with different Ce content used in preparation of metal monolithic catalysts were prepared by the impregnation method using an aqueous solution of cerium nitrite ($Ce(NO_3)_3 \cdot 6H_2O$). The catalyst samples were dried at room temperature and then calcined at 600 °C for 4 h in air. The above prepared Ce/SBA-15 samples powder were mixed with a sol made from boehmite. The nitrate solution was added into the mixture, then the mixture was vigorously stirred for *ca*. 10 h, finally the Ce/SBA-15 slurry was obtained.

The monolithic supports (Al_2O_3/FeCrAl) were prepared according to the method described in the literature [16]. The monolithic supports were dipped into the above Ce/SBA-15 slurry, withdrawn at a constant speed of 3 cm/min, and dried in air, and thereafter at 120 °C for 3 h, and then calcined at 500 °C for 4 h. Finally, the Ce/SBA-15/Al_2O_3/FeCrAl monolithic catalysts were obtained. If a higher loading is required, the coating procedure should be repeated. For the monolithic catalysts, the weight of SBA-15/Al_2O_3 wash coat layers is ca. 11.5 wt% in terms of the catalyst weight including FeCrAl support, and the loadings of Ce/SBA-15 is ca. 6.7 wt% in terms of the catalyst weight not including the FeCrAl support.

2.2 Catalyst Characterization

X-ray powder diffraction (XRD) patterns of the samples were performed with a Bruker D8 diffractometer using Cu Ka radiation at following operation condition: 40 kV and 30 mA in 2θ range of 0.5–5° and 40 kV and 40 mA in 2θ range of 10–80°.

N_2 sorption isotherms were obtained at liquid nitrogen temperature with a Thermo Electron Corporation Sorptomatic 1990 instrument. The samples were degassed at 200 °C under vacuum for 5 h, and the specific surface area of the samples was determined using the Brunauer–Emmett–Teller (BET) method. The pore volume and pore size distribution were derived from the desorption profiles of the isotherms using the Barrett–Joyner–Halanda (BJH) method.

X-ray photoelectron spectroscopy (XPS) experiments were carried out on an Escalab 250 instrument (Thermo Electron Corporation) using Al Kα as the exciting radiation at constant pass energy of 50 eV. Binding energies were calibrated by using the carbon present as a contaminant (C1s = 285.0 eV). The surface atomic compositions of all samples were calculated from photoelectron peak areas for each element after correcting for instrument parameters.

Temperature programed reduction (TPR) experiments were performed using a Thermo Electron Corporation TPD/R/O 1100 series catalytic surfaces analyzer equipped with a TCD detector. Fresh catalysts were preheated with 10 vol% O_2/He mixture heating 10 °C/min up to 600 °C and hold for 120 min, then cooling in flowing N_2 down to room temperature, and thereafter reduced with 5 vol% H_2/N_2 mixture heating 10 °C/min up to 900 °C. For the used and regenerated 10 wt% Ce/SBA-15/Al_2O_3/FeCrAl catalyst, the TPR experiment was performed without being pretreated in the 10 vol% O_2/He atmosphere. Water produced by the sample reduction was condensed in a cold trap before reaching the detectors. Only H_2 was detected in the outlet gas confirming the effectiveness of the cold trap.

2.3 Catalytic Reaction

The ODH of ethane with CO_2 was carried out using a fixed-bed flow-type quartz reactor (i.d., 6 mm; length, 300 mm) under atmospheric pressure. The test was performed with cylindrical monolithic catalysts, which were made up of several cylinders in different diameter and 50 mm in length. Prior to the test, the catalysts were pretreated at 600 °C in a flow of oxygen (O_2, 5 ml/min) for 1 h, and then cooling in flowing argon down to room temperature. Reactant gases, C_2H_6 (the flow rate is 2 ml/min) and CO_2

or Ar (the flow rate is 8 ml/min) were co-fed into the reactor. The gas hourly space velocity (GHSV) is 6,000 ml/g h and the ratio of the $V_{CO_2 \text{ or } Ar}/V_{C_2H_6}$ is 4.0. The velocities of reactant gases were controlled by mass flow controllers (Seven Star D07). The reaction temperature was controlled with a thermocouple attached to the outer wall of the reactor at a position corresponding to the center of the catalytic bed. The apparent activation energy of the catalysts for the ODH of ethane were conducted with significantly low conversions which were usually controlled to be significantly lower than those defined by thermodynamic equilibrium by adjusting GHSV. Rate limitation by external and internal mass transfer under differential conditions proved to negligible by applying suitable experimental criteria. The outlet products were analyzed after the reaction for 30 min by an online GC-4000A gas chromatograph (Beijing East & West Electronics Institute, China) equipped with a 3 mm × 3 m stainless steel column packed with Poropak Q using He as a carrier gas. The calculations of ethane conversion and selectivity for ethylene and methane were based on total carbon balance as follows equations:

$$C_2H_6 conversion = 1 - \frac{2 \times n_{C_2H_6}}{2 \times n_{C_2H_6} + 2 \times n_{C_2H_4} + n_{CH_4}}$$

$$CO_2 conversion = 1 - \frac{n_{CO_2}}{(n_{CO_2} + n_{CO})}$$

$$C_2H_4 selectivity = \frac{2 \times n_{C_2H_4}}{2 \times n_{C_2H_4} + n_{CH_4}}$$

The calculations do not consider the conversion of ethane to coke, as its instantaneous formation is time dependent and difficult to estimate.

3 Results and Discussion

3.1 XRD

The wide-angle XRD patterns of the cleaned FeCrAl alloy, pre-oxidized FeCrAl alloy, SBA-15/Al_2O_3/FeCrAl support and the Ce/SBA-15/Al_2O_3/FeCrAl monolithic catalysts are shown in Fig. 1. The characteristic peaks of FeCr (2θ at 44.3 and 64.6°) are observed in the diffraction pattern of the cleaned FeCrAl foil (Fig. 1a). After the heat treatment at 950 °C for 15 h, besides the characteristic peaks of FeCr, the peaks assigned to α-Al_2O_3 which appear at 2θ = 25.5, 35.0, 37.6, 43.2, 52.4, 57.3, 66.3, and 68.0° are detected on the FeCrAl surface. This indicates that the segregation of an alumina layer on the FeCrAl surface occurred in heat treatment process. The presence of the α-Al_2O_3 layer can improve the adhesion between subsequent wash coat layers and the FeCrAl support [17].

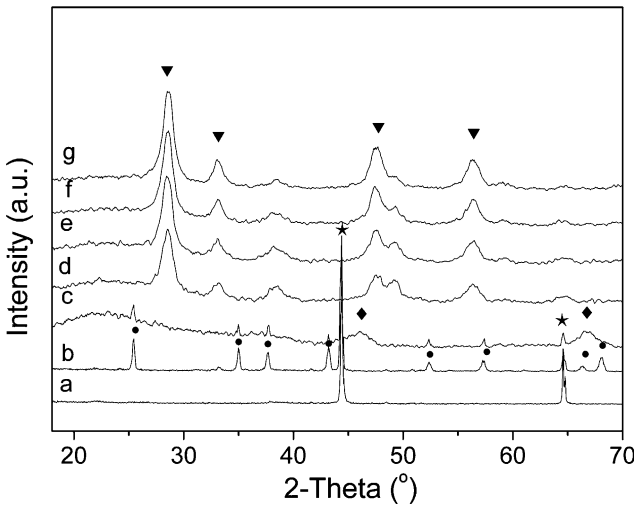

Fig. 1 Wide-angle XRD patterns of (**a**) FeCrAl; (**b**) FeCrAl pre-oxidized at 950 °C; (**c**) SBA-15/Al_2O_3/FeCrAl; (**d**) 5.0% Ce/SBA-15/Al_2O_3/FeCrAl; (**e**) 7.5% Ce/SBA-15/Al_2O_3/FeCrAl; (**f**) 10% Ce/SBA-15/Al_2O_3/FeCrAl; (**g**) 12.5% Ce/SBA-15/Al_2O_3/FeCrAl; (●): α-Al_2O_3; (◆): γ-Al_2O_3; (★): FeCr; (▼): CeO_2

After coating the heat-treated FeCrAl support with SBA-15/Al_2O_3 wash coat, besides the characteristic peaks of FeCr and α-Al_2O_3, those of γ-Al_2O_3 at 46.1 and 66.7° are also observed (Fig. 1c).

For the Ce/SBA-15/Al_2O_3/FeCrAl monolithic catalysts (Fig. 1d–g), it can be observed that the XRD patterns of all the monolithic catalysts are very similar, showing diffraction peaks at 2θ scale followed by 28.5, 32.9, 47.4, and 56.4° corresponding to the (111), (200), (220), and (311) planes, which is the characteristic of cubic, fluorite structure of CeO_2 [9]. Although the intensity of the CeO_2 diffraction peaks increases with the increasing Ce content, the full width at half maximum (FWHM) of the peak at 28.5° does not became wide. This suggests that the CeO_2 particles are introduced into the SBA-15 mesoporous silica, and the CeO_2 particles are in a nanoscale. The average particle size of CeO_2 particles, calculated from the Scherrer equation using the characteristic peak at 28.5°, is about 7.7 nm.

The small-angle XRD patterns of SBA-15, SBA-15/Al_2O_3/FeCrAl support and the Ce/SBA-15/Al_2O_3/FeCrAl monolithic catalysts are presented in Fig. 2. The SBA-15 support (Fig. 2a) shows three well-resolved diffraction peaks in the 2θ range 0.7–2°, corresponding to the diffraction of (100), (110), and (200) planes, and being characteristic of the hexagonally ordered structure of SBA-15 [7]. When SBA-15/Al_2O_3 wash coat is coated onto the FeCrAl support (Fig. 2b), the d_{100} peak shifts to higher angle and attenuates in intensity, suggesting that Al_2O_3 and FeCrAl affect the hexagonally ordered structure of SBA-15. After loading of Ce species on the support, the intensities of these peaks further decreases and the 2θ shifts to

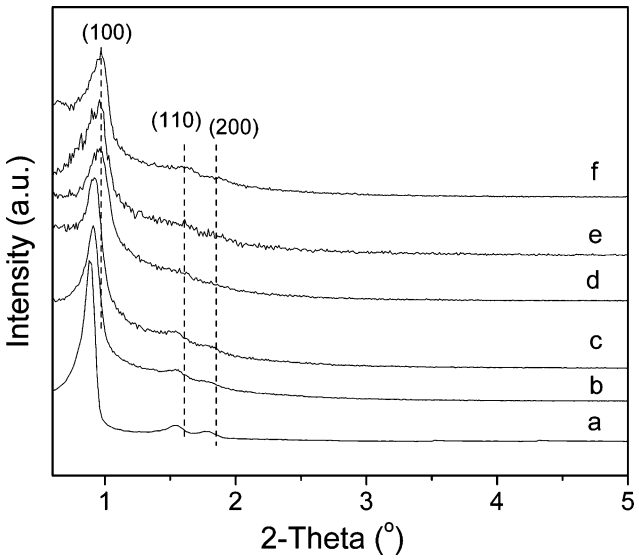

Fig. 2 Small-angle XRD patterns of (**a**) SBA-15; (**b**) SBA-15/Al_2O_3/FeCrAl; (**c**) 5.0% Ce/SBA-15/Al_2O_3/FeCrAl; (**d**) 7.5% Ce/SBA-15/Al_2O_3/FeCrAl; (**e**) 10% Ce/SBA-15/Al_2O_3/FeCrAl; (**f**) 12.5% Ce/SBA-15/Al_2O_3/FeCrAl

higher angles with increasing Ce content (Fig. 2c–f). This indicates that when CeO_2 is introduced into the SBA-15, it declines the organization of the mesoporous structure.

3.2 N_2 Adsorption–Desorption

N_2 adsorption–desorption isotherms and the pore size distributions of the SBA-15/Al_2O_3/FeCrAl support and Ce-based monolithic catalysts are shown in Fig. 3. The corresponding textural properties are given in Table 1. As shown in Fig. 3, the isotherm of the SBA-15/Al_2O_3/FeCrAl

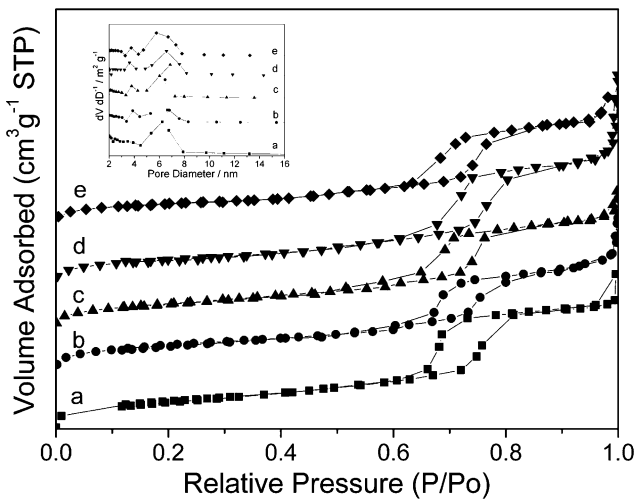

Fig. 3 N_2 adsorption–desorption isotherm and pore size distribution of the samples: (**a**) SBA-15/Al_2O_3/FeCrAl; (**b**) 5.0% Ce/SBA-15/Al_2O_3/FeCrAl; (**c**) 7.5% Ce/SBA-15/Al_2O_3/FeCrAl; (**d**)10% Ce/SBA-15/Al_2O_3/FeCrAl; (**e**) 12.5% Ce/SBA-15/Al_2O_3/FeCrAl

support exhibits a type IV isotherm with H1-type hysteresis, which is typical of mesoporous materials with one-dimensional cylindrical channels [7]. The sharp inflection between the relative pressure $P/P_0 = 0.6–0.8$ observed in the isotherm corresponds to capillary condensation within uniform mesopores. After Ce loading, all the isotherms of the Ce-based monolithic catalysts are similar with that of SBA-15/Al_2O_3/FeCrAl support. This suggests that the hexagonally ordered structure of SBA-15 remains in the monolithic catalysts. Whereas the hysteresis inflection is less sharp indicating that the pore size of the monolithic catalyst is less ordered and uniform compared to that of the SBA-15/Al_2O_3/FeCrAl support. This indicates that the loading of Ce affects the mesoporous structure of SBA-15. The result is in accordance with the above low-angle XRD results.

Table 1 shows the physical properties of the SBA-15/Al_2O_3/FeCrAl support and Ce-based monolithic catalysts. The SBA-15/Al_2O_3/FeCrAl support displays a BET specific surface area (S_{BET}) of 45.1 m^2/g and a 6.7 nm pore diameter (D_{BJH}). After Ce loading, the S_{BET} value decreases gradually. This can be attributed to the presence of extra-framework CeO_2 with lower specific surface area on the pore walls and/or the partial blockage of the SBA-15 pores, and is consistent with the decrease in pore volume (see Table 1) of the Ce/SBA-Al_2O_3/FeCrAl samples with increasing Ce content. In addition, two type pores are observed at ca. 3.9 nm and ca. 6.5 nm. The former type pore may be caused by the insertion of the Ce component into the channels of SBA-15 which partly block the channels. The latter is the banana-like SBA-15 with ordered pores [18].

3.3 H_2-TPR

Figure 4 shows the H_2-TPR results of the Ce-based monolithic catalysts with different Ce content. The CeO_2 shows a reduction peak at ca. 600 °C, which is attributed to the reduction of surface Ce^{4+} to Ce^{3+} species. For all the Ce-based monolithic catalysts, there is a wide reduction peak centered at ca. 400 °C indicative of the reduction of surface Ce^{4+} to Ce^{3+}, suggesting that CeO_2 can be only partially reduced under the experimental conditions employed in this work. This is consistent with the results reported by other authors [19, 20]. The peak temperature has a obviously decrease comparing with that of CeO_2. This may be caused by the interaction of the support and Ce species, and the interaction increases the reducibility of Ce species in the monolithic catalysts. With increasing Ce content, the reaction peak shifts to higher temperature. This behavior can be ascribed to the formation of more Ce^{3+} phase with higher Ce loading, which would hinder the reduction of Ce^{4+} species. The formation of more Ce^{3+} phase can be proved by the following XPS results. The

Table 1 Textural and structural characteristics and TPR date of the monolithic catalysts

Samples	S_{BET} (m^2/g)	V_p (cm^3/g)	D_{BJH} (nm)	T_{peak} (°C)	H_2 consumption (μmol/g cat)	Ce^{4+} (μmol/g cat)
SBA-15/Al_2O_3/FeCrAl	45.1	0.07	6.7	–	–	–
5.0% Ce/SBA-15/Al_2O_3/FeCrAl	41.9	0.07	3.9, 6.5	400	29.1	58.2
7.5% Ce/SBA-15/Al_2O_3/FeCrAl	39.4	0.07	3.8, 6.6	400	36.3	72.6
10% Ce/SBA-15/Al_2O_3/FeCrAl	37.2	0.06	3.6, 6.6	409	46.4	92.8
12.5% Ce/SBA-15/Al_2O_3/FeCrAl	32.2	0.06	3.8, 5.8	409	42.6	85.2

TPR data and the amount of Ce^{4+} in the monolithic catalysts calculated from H_2 consumption (according reaction: $2CeO_2 + H_2 = Ce_2O_3 + H_2O$) are summarized in Table 1. It is observed that the amount of Ce^{4+} increases with higher Ce loading and reaches maximum (92.8 μmol/g cat) in the 10% Ce loading monolithic catalyst. Further increasing Ce content, the amount of Ce^{4+} has a slight decrease. It is probable that the higher Ce loading easily results in the formation of nonstoichiometric CeO_2 (CeO_{2-x}, $2 > x > 1.5$). Consequently, the Ce-based monolithic catalysts consume less H_2 during H_2-TPR process.

3.4 XPS

The XPS cerium spectra of the Ce-based monolithic catalysts with various cerium contents are shown in Fig. 5. Several authors had reported the complexity of the Ce3d spectra in Ce-based materials [21–23]. The binding energy Ce3d of Ce-based monolithic catalyst with different Ce content, for the characteristic Ce^{4+} component overlaps that corresponding to Ce^{3+}. However, the deconvolution of the spectra showed well-defined peaks that enabled the estimation of the relative contribution by the Ce^{4+} (CeO_2) and Ce^{3+} (Ce_2O_3) species (Table 2 and Fig. 5). As for the monolithic catalyst samples, the $3d_{5/2}$ level energies around 888.2–888.6 eV assigned to Ce^{3+} as well as the peaks corresponding to the binding energies at 882.1–882.4 eV and 898.0–898.3 eV assigned to Ce^{4+} are observed [24, 25]. The Ce^{4+} assignment is confirmed by the presence of the satellite structure at 916.3–916.7 eV [26], which is typical of tetravalent cerium species.

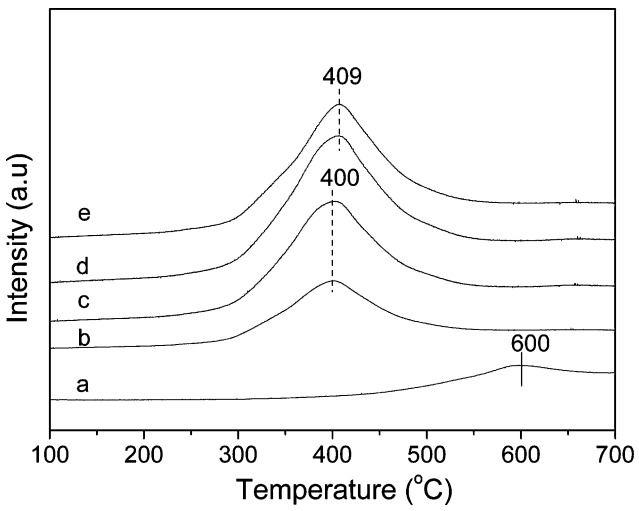

Fig. 4 TPR profiles of the samples: (**a**) CeO_2; (**b**) 5.0% Ce/SBA-15/Al_2O_3/FeCrAl; (**c**) 7.5% Ce/SBA-15/Al_2O_3/FeCrAl; (**d**) 10% Ce/SBA-15/Al_2O_3/FeCrAl; (**e**) 12.5% Ce/SBA-15/Al_2O_3/FeCrAl

The proportions of Ce^{4+} and Ce^{3+} in the Ce-based monolithic catalysts are shown in Table 2. The proportion of Ce^{4+}/Ce^{3+} varies with the loading of Ce species in the monolithic catalysts. With increasing Ce content form 5.0 to 10.0%, the value of Ce^{4+}/Ce^{3+} increases from 1.94 to 2.30. However, further increasing Ce content to 12.5%, the value of Ce^{4+}/Ce^{3+} has a slight decrease. This result indicates that the more Ce^{3+} phase formed on the Ce-based monolithic catalysts when the Ce content is above 10.0%. This is consistent with the results of H_2-TPR.

3.5 Catalytic Activity

The dehydrogenation of ethane over the Ce-based monolithic catalysts in the presence of CO_2 and Ar atmosphere are evaluated and the results are shown in Table 3. The SBA-15/Al_2O_3/FeCrAl support shows negligible ethane and carbon dioxide conversions in reaction conditions. For the ODH of ethane reaction, in the presence of CO_2 atmosphere, the major reaction product is C_2H_4, and the minor products are CH_4, CO, H_2 and H_2O. Whereas, in the presence of Ar atmosphere, the above products are also detected except for CO and H_2O components. The appearance of CO in the products suggests that CO_2 participates in reaction and is converted into CO. The CO can be formed through the reverse water-gas shift reaction and/or the direct reaction of CO_2 and ethane [27]. It is also observed that for the Ce-based monolithic catalysts, in the CO_2 atmosphere, the ethane conversion is obviously higher than that in the Ar atmosphere. This indicates that CO_2 plays a positive role in the ODH of ethane reaction.

For the Ce-based monolithic catalysts, the catalytic activities vary with Ce loading. In the CO_2 atmosphere, with increasing Ce loading, the ethane and CO_2 conversions on Ce-based monolithic catalysts first increase and

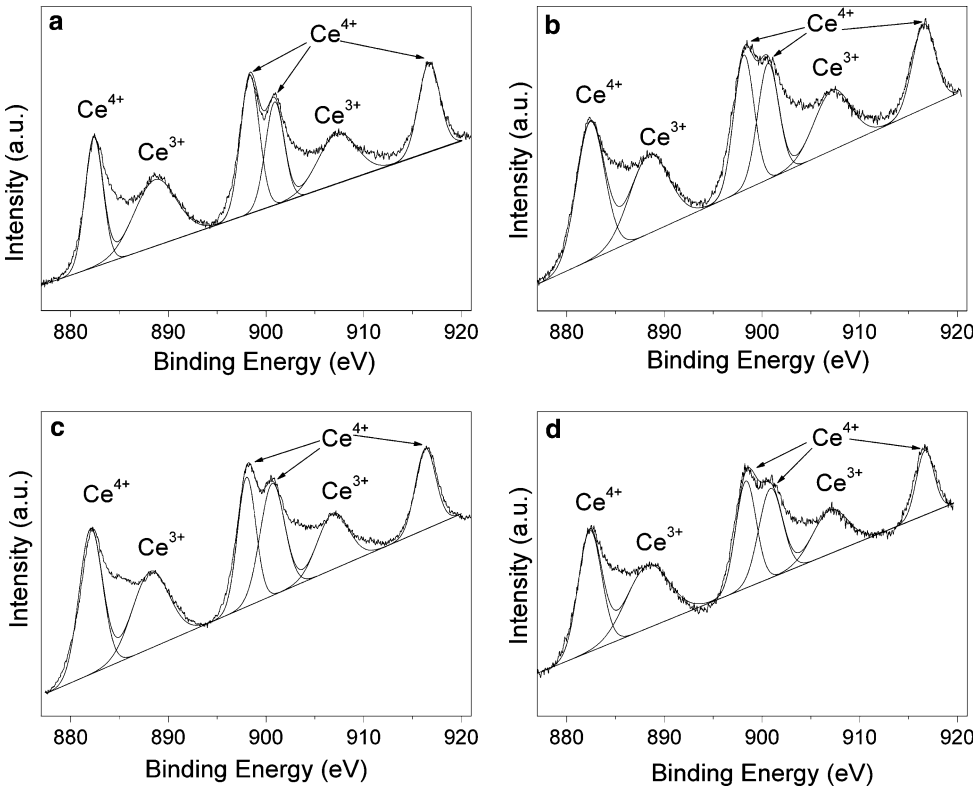

Fig. 5 XPS spectra of Ce3d over the catalysts: (**a**) 5.0% Ce/SBA-15/Al_2O_3/FeCrAl; (**b**) 7.5% Ce/SBA-15/Al_2O_3/FeCrAl; (**c**) 10% Ce/SBA-15/Al_2O_3/FeCrAl; (**d**) 12.5% Ce/SBA-15/Al_2O_3/FeCrAl

Table 2 Surface concentration of the Ce elements

Catalyst	Ce (%)	Ce^{4+} BE (eV)				Ce^{3+} BE (eV)			Ce^{4+}/Ce^{3+}
5.0% Ce/SBA-15/Al_2O_3/FeCrAl	0.94	882.3[a] (17.6)[b]	898.3 (19.5)	900.9 (14.4)	916.7 (14.5)	888.6 (20.1)	907.3 (13.9)	1.94
7.5% Ce/SBA-15/Al_2O_3/FeCrAl	0.99	882.4 (24.0)	898.1 (16.2)	900.6 (15.1)	916.5 (12.2)	888.4 (18.9)	907.2 (13.6)	2.08
10% Ce/SBA-15/Al_2O_3/FeCrAl	1.17	882.1 (23.4)	898.0 (16.4)	900.6 (18.5)	916.3 (11.4)	888.2 (18.7)	906.8 (11.7)	2.30
12.5% Ce/SBA-15/Al_2O_3/FeCrAl	1.25	882.4 (23.2)	898.3 (18.3)	900.9 (17.2)	916.7 (9.8)	888.3 (20.2)	907.0 (11.3)	2.17

[a] The binding energy (BE) values were corrected using the C1s peak at 285.0 eV

[b] The value in the bracket means the relative content from Ce 3d

Table 3 Activity of Ce-based monolithic catalysts for the ethane dehydrogenation

Samples	In the presence of CO_2						In the presence of Ar				
	Conv. (%)		Sel. (%)		Yield C_2H_4 (%)	Ep kJ/mol	Conv. (%)	Sel. (%)		Yield C_2H_4 (%)	Ep kJ/mol
	C_2H_6	CO_2	C_2H_4	CH_4			C_2H_6	C_2H_4	CH_4		
SBA-15/Al_2O_3/FeCrAl	4.9	0.1	94.9	5.0	4.7	–	4.5	93.2	6.8	4.2	–
5.0% Ce/SBA-15/Al_2O_3/FeCrAl	54.1	9.4	89.0	11.0	48.2	134.5	39.7	91.5	9.5	36.3	161.2
7.5% Ce/SBA-15/Al_2O_3/FeCrAl	57.4	9.7	88.8	11.2	50.1	124.8	41.5	90.1	9.9	37.4	157.7
10% Ce/SBA-15/Al_2O_3/FeCrAl	63.9	10.5	87.2	12.8	55.7	118.1	43.6	89.4	11.6	38.5	149.6
12.5% Ce/SBA-15/Al_2O_3/FeCrAl	59.7	9.2	88.7	12.3	53.0	129.1	43.8	83.2	12.8	36.4	147.0

Reaction conditions: GHSV = 6,000 ml/g h, $V_{CO_2orAr}/V_{C_2H_6} = 4.0$, T = 750 °C

then decrease. The maximum C_2H_6 and CO_2 conversions are 63.9 and 10.5%, respectively, which can be achieved on the 10% Ce loading monolithic catalyst. In the Ar atmosphere, although the ethane conversion slightly increase with increasing Ce content, the maximum yield of C_2H_4 also can be obtained on the 10% Ce loading monolithic catalyst. In the ODH of ethane with CO_2 over Ce-based monolithic catalyst, a redox mechanism was suggested in

the presence of CO_2 [28]. Suppose the catalytic reaction is carried out via the reduction of the catalyst by C_2H_6 and its oxidation by CO_2, in a redox cycle similar to that of Mars–van Krevelen, in which Ce^{3+} produced by the reduction of Ce^{4+} by the alkane, was reoxidized by CO_2. The key point of this hypothesis, the oxidation of partially reduced ceria by CO_2, has been evidenced by Sharma et al. [29] who examined the redox properties of Pd/ceria using CO_2 as oxidant, and it was evidenced that ceria can be partially reduced by CO and partially reoxidized by CO_2. The redox cycle process can be denoted as follows:

$$Ce_2O_3 + CO_2 \rightarrow 2CeO_2 + CO$$

Which is thermodynamically favorable at 298 K as ΔG^0 is −85.8 kJ/mol and ΔH^0 is −96.8 kJ/mol. Therefore, the redox properties and the ability to store and release oxygen of CeO_2 are also seen when CO_2 is used as an oxidant in the ODH of ethane with CO_2.

Figure 6 presents the variation of the catalytic performance with the reaction temperature. The conversion of ethane and CO_2 increases with raising temperature. The ethylene selectivity decreases and the methane selectivity increases within the studied temperature range. This effect should be attributed to an acceleration of the side reactions at high temperature.

Combining the above XPS results and the catalytic activity of ODH reaction, it can be noticed that the values of Ce^{4+}/Ce^{3+} have a good correlation with the ethane conversion and ethylene yield. The Ce-based monolithic catalyst with high Ce^{4+}/Ce^{3+} value has high ethane conversion and ethylene yield. So, cerium species with the high oxidation state may be playing a key role to higher catalytic activity during the ODH of ethane. The TPR results also indicate the Ce-based monolithic catalyst with more Ce^{4+} species has higher catalytic activity for ODH of ethane with CO_2.

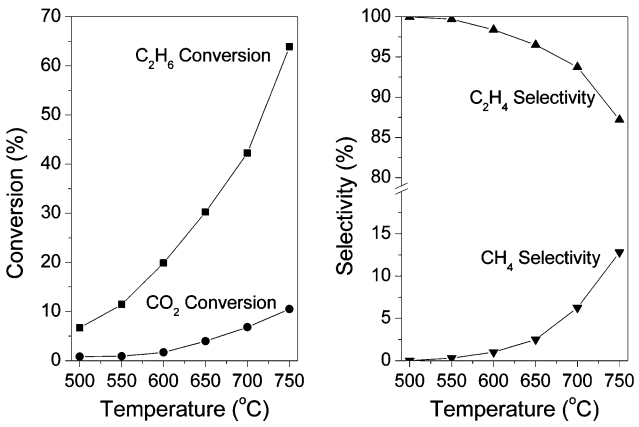

Fig. 6 Variation of catalytic performances of 10% Ce/SBA-15/Al_2O_3/FeCrAl with reaction temperature in ODH of ethane with CO_2 Reaction conditions: GHSV = 6,000 ml/g h, $V_{CO_2}/V_{C_2H_6} = 4.0$

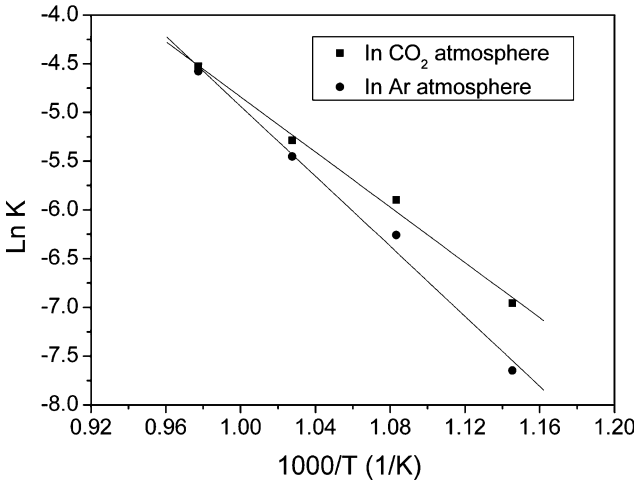

Fig. 7 Arrhenius plots for ethane dehydrogenation over 10% Ce/SBA-15/Al_2O_3/FeCrAl catalyst in CO_2 or Ar atmosphere. The K is reaction velocity constant. Reaction conditions: GHSV = 9,600 ml/g h, $V_{CO_2orAr}/V_{C_2H_6} = 4.0$; the plots include data from about 5 to 25% conversion

The reactivity of the catalysts also is reflected in the apparent activation energy (Ep), derived from kinetic measurements. The apparent activation energy for the Ce-based monolithic catalyst under study is calculated from Arrhenius plots (such as Fig. 7) for ethane consumption rates. The values obtained in this work are shown in Table 3. In the CO_2 atmosphere, it can be known that the Ce-based monolithic catalysts with more Ce^{4+} species or high Ce^{4+}/Ce^{3+} values (as shown by TPR and XPS results) show the low Ep values. This indicates that Ce^{4+} species has higher catalytic activity for ODH of ethane with CO_2 than that of Ce^{3+} species in the Ce-based monolithic catalysts. In other words, for the different Ce content catalysts, the difference of the apparent activation energy is caused by the different Ce^{4+}/Ce^{3+} values or the amount of Ce^{4+} species in the Ce-based monolithic catalysts.

It also can be seen that, for the same catalyst, it shows different apparent activation energy in the CO_2 and Ar atmosphere. The difference in the apparent activation energy suggests that the reaction pathway over the Ce-based monolithic catalysts is different. In the CO_2 atmosphere, CO_2 can be used as a soft oxidant, and the redox cycle is realized easily at the reaction conditions. Thus the main pathway should be oxidative dehydrogenation. In contrast, in the Ar atmosphere, Ar is an inert gas, and the main pathway is deduced to be simple dehydrogenation on the monolithic catalysts.

3.6 Deactivation and Regeneration

For the ODH reaction, the catalyst deactivation is still an involved problem and the industry applications of catalysts

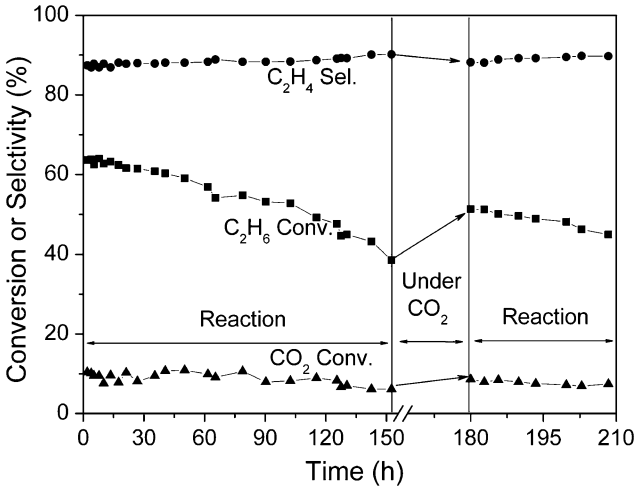

Fig. 8 Deactivation and regeneration of 10% Ce/SBA-15/Al_2O_3/FeCrAl monolithic catalyst; GHSV = 6,000 ml/g h, $V_{CO_2}/V_{C_2H_6} = 4$, T = 750 °C

are restricted due to poor stability of catalysts. Therefore, in this study, the deactivation and regeneration by CO_2 of Ce-based monolithic catalysts were investigated. As shown in Fig. 8, the catalytic activity of the 10% Ce content monolithic catalyst decreases gradually with increasing reaction time. The conversion of ethane decreases from 63.7 to 38.5% after 152 h reaction. The XPS result indicates that the intensity of peaks at 882.9, 898.9, and 901.9 eV corresponding to the Ce^{4+} oxidation state has a relative decrease after the 152 h reaction (Fig. 9). The value of Ce^{4+}/Ce^{3+} decreases from 2.30 (before reaction) to 1.47 (after 152 h reaction, see Table 4). These results indicate that the deactivation of the Ce-based monolithic catalyst may be associated with the reduction of high oxidation state cerium (Ce^{4+}) species. This result also is supported by the TPR date in which the amount of Ce^{4+} calculated from H_2 consumption decreases from 92.8 μmol/g cat (before reaction) to 17.6 μmol/g cat (after 152 h reaction, see Table 4). In addition, the carbon deposition may be another reason for the deactivation of the catalyst.

After the reaction for 152 h, the gas flow of the C_2H_6 and CO_2 mixture was replaced with a gas flow of pure CO_2 at 10 ml/min to regenerate the catalyst for 24 h. It can be noted the ethane conversion of the Ce-based monolithic catalyst recovers from 38.5 to 51.3%, which is insufficient recovery. The XPS result indicates the value of the Ce^{4+}/Ce^{3+} also insufficiently recover from 1.47 (after reaction) to 1.80 (after regeneration, see Table 4 and Fig. 9). From TPR result (Fig. 10), it can be seen that, before reaction, the reduction peak at ca. 409 °C is attributed to the reduction of Ce^{4+} to Ce^{3+} species. After reaction, the reduction peak becomes smaller, almost disappearing over the Ce-base monolithic catalyst, suggesting that most Ce^{4+} species are reduced to Ce^{3+} species in ODH reaction. After regenerated with CO_2 at 750 °C for 24 h, the reduction peak of Ce^{4+} species appears again. The amount of Ce^{4+} species recovers from 17.6 μmol/g cat. (after reaction) to 57.7 μmol/g cat. (after regeneration, see Table 4). At the same time, the maximum temperature (T_{peak}) of the reduction peak shifts to higher temperature region after regeneration. This suggests the interaction between Ce species and support has changed in the reaction and regeneration treatment.

On the basis of the activity results and the above-mentioned analyzes, we suggest the following reaction scheme for the ODH of ethane with CO_2 over the active Ce catalysts. The reaction proceeds through a redox cycle involving Ce^{4+} and Ce^{3+} species. In fact, a Ce redox cycle can be observed at as low as 623 K [29], which is lower than the temperature of the ethane dehydrogenation in this study work. The XPS and TPR analyzes demonstrated that in the reaction over the Ce-based monolithic catalyst, a Ce^{4+} species was reduced to Ce^{3+} by ethane treatment, and CO_2 treatment led to reoxidation to Ce^{4+} species. On the basis of the current results, we believe that a high oxidation state Ce species is effective for the ODH reaction. Indeed, the reduction of the species to Ce^{3+} was demonstrated by TPR analysis. A Ce redox cycle (Scheme 1) may occur during the ODH of ethane in the presence of CO_2 atmosphere.

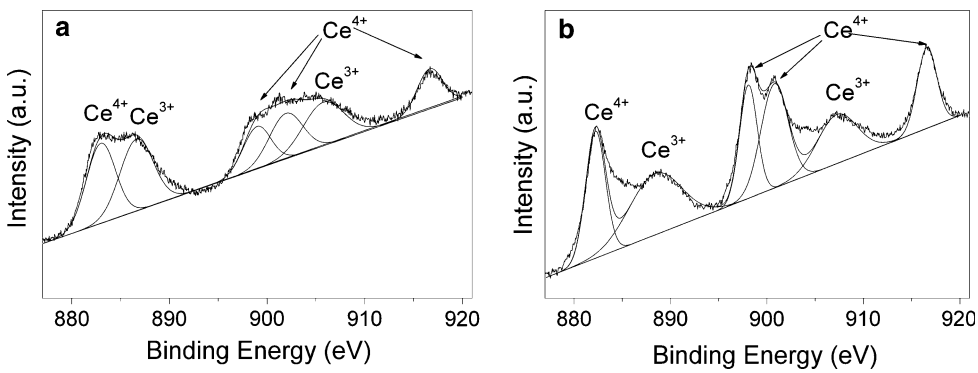

Fig. 9 XPS spectra of Ce 3d over the 10% Ce/SBA-15/Al_2O_3/FeCrAl sample: (**a**) After reaction (at 750 °C for 152 h); (**b**) After Regeneration (Regenerated by CO_2 at 750 °C for 24 h)

Table 4 Surface concentration of Ce elements and TPR data for 10% Ce monolithic catalyst

Catalyst	Ce (%)	Ce^{4+} BE (eV)			Ce^{3+} BE (eV)			Ce^{4+}/Ce^{3+}	T_{peak} (°C)	Ce^{4+} (μ mol/g cat)
After reaction[a]	1.02	882.9[b] (23.1)[c]	898.9 (11.5)	901.9 (14.7)	916.7 (10.2)	886.6 (23.4)	905.8 (17.1)	1.47	409, 557	17.6
After regeneration[d]	1.08	882.2 (18.2)	898.1 (14.5)	900.8 (19.9)	916.6 (11.7)	888.4 (22.2)	907.3 (13.6)	1.80	444	57.7

[a] After reaction at 750 °C for 152 h

[b] The binding energy (BE) values were corrected using the C1s peak at 285.0 eV

[c] The value in the bracket means the relative content from Ce 3d

[d] Which was regenerated by CO_2 at 750 °C for 24 h

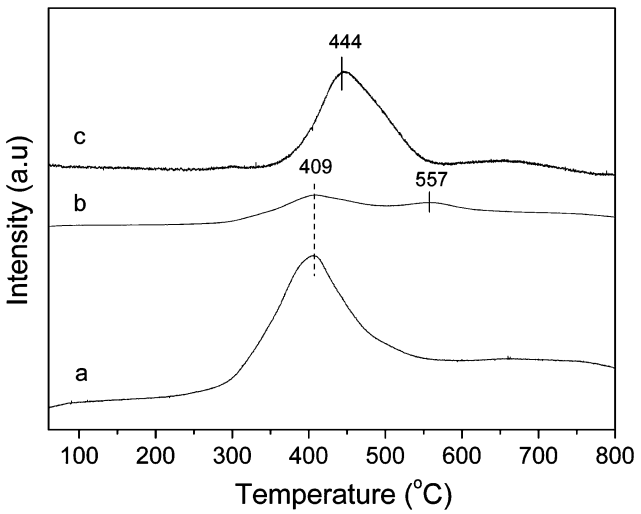

Fig. 10 TPR profiles of the 10% Ce/SBA-15/Al_2O_3/FeCrAl samples: (**a**) Before reaction; (**b**) After reaction at 750 °C for 152 h; (**c**) After regenerated by CO_2 at 750 °C for 24 h

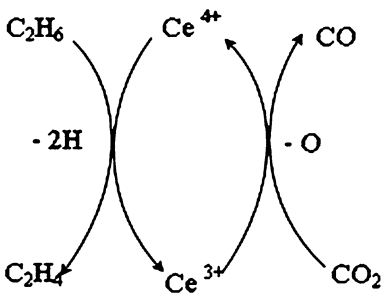

Scheme 1 Redox cycle of active Ce species on monolithic catalyst surface

4 Conclusions

Ce-based monolithic catalysts with different cerium content were prepared. All the monolithic catalysts display the hexagonally ordered structure of SBA-15, and the loading of Ce species decline the organization of the mesoporous structure. The Ce-based monolithic catalysts show excellent catalytic activity for the ODH of ethane with CO_2. In the monolithic catalysts, the high oxidation state Ce^{4+} species has higher catalytic activity than the Ce^{3+} species for the ODH reaction. The Ce^{4+} species can be reduced to Ce^{3+} species by ethane dehydrogenation process, and the reduced Ce species also can be reoxidized to the Ce^{4+} species by CO_2 treatment. The Ce redox cycle is important for the high catalytic activity for the ODH of ethane with CO_2 reaction.

Acknowledgments Financial funds from the National Natural Science Foundation of China (Project Nos. 20473009) and the National Basic Research Program of China (Project No. 2005CB221405) are gratefully acknowledged.

References

1. Cavani F, Balarini N, Cericola A (2007) Catal Today 127:113
2. Weckhuysen BM, Schoonheydt RA (1999) Catal Today 51:223
3. Blasco T, Lopez-Nieto JM (1997) Appl Catal A 157:117
4. Mamedov EA, Cortes Corberan V (1995) Appl Catal A 127:1
5. Lemonidou AA, Nalbandian L, Vasalos IA (2000) Catal Today 46:333
6. Grzybowska-Swierkosz B (2002) Topics Catal 21:35
7. Zhao D, Feng J, Huo Q, Melosh N, Fredrickson GH, Chmelka BF, Stucky GD (1998) Science 279:548
8. Hartmann M, Vinu A (2002) Langmuir 18:8010
9. Burri DR, Choi KM, Lee JH, Han DS, Park SE (2007) Catal Commun 8:43
10. Włoch E, Łukaszczyk A, Żurek Z, Sulikowski B (2006) Catal Today 114:231
11. Hou ZY, Yashima T (2004) Appl Catal A 261:205
12. Roy S, Heibel AK, Liu W, Boger T (2004) Chem Eng Sci 59:957
13. Groppi G, Ibashil W, Tronconi E, Forzatti P (2001) Chem Eng J 82:57
14. Liu H, Zhao J, Li C, Ji S (2005) Catal Today 105:401
15. Mei H, Li C, Liu H (2005) Catal Today 105:689
16. Wang K, Li X, Ji S, Huang B, Li C (2008) ChemSusChem 1:527
17. Wu XD, Weng D, Zhao S, Chen W (2005) Surf Coat Technol 190:434
18. Zhang L, Zhao YH, Dai HX, He H, Au CT (2008) Catal Today 131:42
19. Rocchini E, Trovarelli A, Llorca J, Graham GW, Weber WH, Maciejewski M, Baiker A (2000) J Catal 194:461
20. Dai Q, Wang X, Lu G (2008) Appl Catal B 81:192
21. Burroughs P, Hammett A, Orchard AF, Thornton G (1976) J Chem Soc. Dalton Trans 17:1686
22. Liu G, Rodriguez JA, Hrbek J, Dvorak J (2001) J Phys Chem B 105:7762

23. Larese C, Cabello Galisteo F, Lopez Granados M, Mariscal R, Fierro JLG, Lambrou PS, Efstathiou AM (2004) J Catal 226:443
24. Pfau A, Schierbaum KD (1994) Surf Sci 321:71
25. Heckert EG, Karakoti AS, Seal S, Self WT (2008) Biomaterials 29:2705
26. Zaki MI, Hussein GAM, Manssur SAA, Ismael HM, Merhemer GAH (1997) Colloid Surf A 127:47
27. Wang S, Murata K, Hayakawa T, Suzuki K (2000) Appl Catal A 196:1
28. Valenzuela RX, Bueno G, Cortés Corberán V, Xu Y, Chen C (1998) Abstracts 215th ACS Nat. Meeting, Dallas, COLL-085
29. Sharma S, Hilaire S, Vohs JM, Gorte RJ, Jen HW (2000) J Catal 190:199